Structural and dynamical properties of guest molecules confined in mesoporous silica materials revealed by NMR

Gerd Buntkowsky,*[a] Hergen Breitzke,[a] Anna Adamczyk,[a] Frank Roelofs,[a] Thomas Emmler,†[b] Egbert Gedat,[b] Bob Grünberg,[b] Yeping Xu,[b] Hans-Heinrich Limbach,[b] Ilja Shenderovich,[b] Anastasia Vyalikh‡[b] and Gerhard Findenegg[c]

Received 15th May 2007, Accepted 14th June 2007
First published as an Advance Article on the web 9th July 2007
DOI: 10.1039/b707322d

In the last fifteen years several novel porous silica materials, which are periodically structured on the mesoscopic length scale, have been synthesized. They are of broad interest for fundamental studies of surface–substrate interactions, for studies of the dynamics of guest molecules in confinement and for studies of the effect of confinement on the structural and thermophysical properties of fluids. Examples of such confinement effects include the change of the freezing and melting points or glass transitions of the confined liquids. These effects are studied by combinations of several NMR techniques, such as ^{15}N- and ^{2}H-solid-state NMR line shape analysis, MAS NMR and NMR diffusometry with physico-chemical characterization techniques such as nitrogen adsorption and small angle diffraction of neutrons or X-rays. This combination does not require crystalline samples or special clean and well defined surfaces such as conventional surface science techniques, but can work with typical ill-defined real world systems. The review discusses, after a short introduction, the salient features of these materials and the applied NMR experiments to give the reader a basic knowledge of the systems and the experiments. The rest of the review then focuses on the structural and dynamical properties of guest molecules confined in the mesoporous silica. It is shown that the confinement into the pores leads to fascinating new features of the guests, which are often not known for their bulk phases. These features depend strongly on the interplay of the their interactions with the silica surface and their mutual interactions.

Introduction

15 years ago a new class of mesoporous silica materials has become available which is characterized by a periodic pore structure although the silica matrix is disordered on an atomic length scale.[1–6] Typical representatives of such periodic mesoporous silica (PMS) materials are MCM-41 and SBA-15, which constitute two-dimensionally hexagonal arrays of cylindrical pores. Owing to the presence of surface silanol groups at the pore walls, these materials can be chemically tailored to various functions.[7] PMS materials opened up fascinating possibilities for new applications in many fields, including catalysis,[8–11] drug delivery or size selective molecular separation.[12] At the same time, these materials are of broad interest for fundamental studies of surface–substrate interactions and of the dynamics of guest molecules in confinement.[13–21]

PMS materials are also very well-suited for fundamental studies of the effect of confinement on the structural and thermophysical properties of fluids. This interest is motivated by the desire to better understand the influence of surface forces and finite-size effects on the behavior of the substrate in the pores.[22] Examples of such confinement effects include the change of the freezing and melting points or glass transitions of the confined liquids.[20,22–25] The change of the melting point is often discussed by the Gibbs–Thomson equation,[26] which predicts a linear dependence of the melting point depression ΔT_m on the inverse pore radius $1/R$:

$$\Delta T_m = T_{m(bulk)} - T_{m(pore)} = \frac{2V_m T_{m(bulk)}(\gamma_{cw} - \gamma_{lw})}{\Delta H_m R} \quad (1)$$

where $T_{m(bulk)}$ is the bulk melting temperature, V_m is the molar volume of the liquid phase, ΔH_m the molar enthalpy of melting, and $(\gamma_{cw} - \gamma_{lw})$ the difference of the surface free energies crystal-wall and liquid-wall, which for the case of complete wetting of the pore walls by the liquid is given by the crystal/liquid interfacial free energy γ_{cl}.[22] A detailed survey for the current state of the theory of melting points is given in the review by Alcoutlabi and McKenna.[27]

[a] *FSU Jena, Institut für Physikalische Chemie, Helmholtzweg 4, 07743 Jena, Germany. E-mail: gerd.buntkowsky@uni-jena.de; Fax: +49 3641 948302*
[b] *Freie Universität Berlin, Institut für Chemie, Takustraße 3, 14195 Berlin, Germany*
[c] *Technische Universität Berlin, Stranski-Laboratorium für Physikalische und Theoretische Chemie, Straße des 17. Juni 124, 10623 Berlin, Germany*
† Present address: GKSS-FZ Geesthacht, D-21502, Geesthacht, Germany.
‡ Present address: IFW Dresden, D-01171 Dresden, Germany.

A melting behavior conforming with eqn (1) or with a modified Gibbs–Thomson equation was indeed found for water[5,28] and other liquids[29] in a series of MCM-41 and SBA-15 materials of 2 to 10 nm pore width.

However, as discussed in detail by the review of McKenna *et al.*,[27] the Gibbs–Thomson equation is not the end of the story. Until now the depression of the melting point in confined media or in particular the change of the glass transition temperature is theoretically not completely understood, despite the fact that even technical systems nowadays are approaching nanometer dimensions. It is therefore necessary to improve our knowledge of how geometrical confinement on the nanometer scale alters the behavior of disordered condensed matter relative to bulk materials. A recent survey about the theoretical modelling and description of fluids confined in nanoporous and mesoporous material is given in the textbook by Schoen and Klapp.[30]

Part of the difficulty in the description of these systems is the complex interplay of interactions between the molecules themselves on the one hand and the molecules and the surface on the other hand. Since the pore diameter is typically a factor 10 to 100 greater than the size of the guest molecules, a substantial fraction of the guest molecules is in direct vicinity of the surface. As a result the two types of interactions are of comparable magnitude. Moreover both types of interactions might have the simple geometry dependence of an electrostatic or dispersion interaction or the complex angular behavior of a strong hydrogen bond.

A deeper understanding of the structure–property relation in these systems, which goes beyond the thermodynamic level, necessitates a detailed characterization of the surface and guest structures inside these pores and their changes. Much progress has been made in the characterization of the pore structure of PMS materials at a mesoscopic length scale by small-angle X-ray diffraction.[31,32] Recently, this method has also been applied to *in situ* studies of the condensation of vapors in the porous matrix,[33,34] and adsorbed surfactant layers in the pore space.[35] For studying the behaviour at a molecular level, the large inner surface area and inner volume of these materials provides the necessary sensitivity to allow a detailed analysis using a variety of NMR technique. A great advantage of NMR techniques is that they do not necessitate special clean and well defined surfaces such as conventional surface science techniques, but can work with the typical ill-defined real world systems, as for example technical silica materials. In particular since NMR is an integral method it is not strongly affected by small concentrations of impurities. NMR techniques allow also the study of modified silica materials, which are prepared for example under low surfactant concentration[36] or functionalized by organic groups.[37] Combining several of these NMR techniques (see Fig. 1) it is possible to reveal the binding situation, the translational and the rotational dynamics of the guest molecules on or near the surface, respectively, inside the pores and the adsorption/desorption kinetics of the guests.[20,38–49] Additional information about dynamic processes inside the pores are obtainable by other NMR methods, as for example the stimulated echo or 2D-exchange NMR are discussed in detail in the textbook[50] and the recent review by Boehmer *et al.*[51]

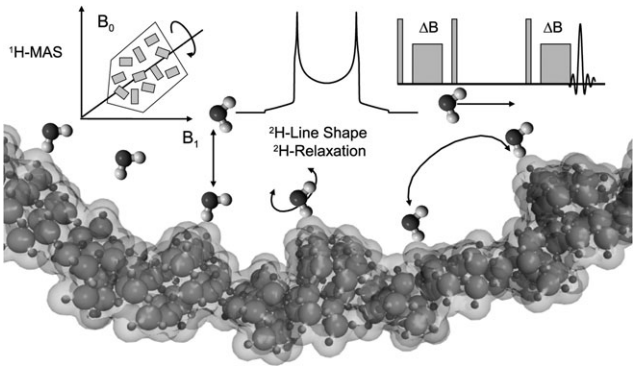

Fig. 1 Overview of the different NMR techniques which are used in this review for the study of the molecular processes in a confined geometry.

The purpose of this short review is to give the reader an overview about the current state of the art in NMR studies of these systems and the underlying NMR methodology for the characterization of these new materials, employing mainly research examples from our group. A deeper discussion of the formation of glasses is beyond the scope of this review. Here the reader is referred to the recent papers by Paul and Smith[52] and Berthier *et al.*[53] and references cited therein.

Materials and methods

Mesoporous silica materials

PMS materials consist of pseudo-crystalline powders, where each crystallite constitutes a large number of more or less parallel cylindrical pores. The silica formation takes place in aqueous media using surfactants or amphiphilic block copolymers as structure-directing agents (template). The pore diameters can be adjusted by the templating agents. Typically, they are between 2 and 4 nm in the case of MCM-41 silicas, and between 5 and 12 nm for SBA-15 silicas.[5] Materials with wider pores (up to 50 nm and more) but nonperiodic structure can be synthesized by similar procedures. After silica formation the templating agents are removed by calcination. The high porosity causes a large inner surface of these materials. Owing to their wide range of pore sizes, they are very versatile molecular sieves. Since the physical properties of their inner surfaces, such as the surface acidity, can be chemically modified,[54,55] mesoporous silica materials are very promising candidates for catalytic applications.

NMR spectroscopy

Nuclear magnetic resonance[56,57] (NMR) is a well known spectroscopic technique which covers a very large range of application areas, due to the multitude of different NMR techniques which are available today. Roughly three principal NMR domains can be distinguished, namely liquid-state NMR spectroscopy,[58] spatially resolved NMR techniques[59–61] and solid-state NMR spectroscopy.[50,62] While the main application of liquid-state NMR spectroscopy refers to the area of chemical and biochemical analysis of liquid or soluble compounds, spatially resolved NMR techniques are primarily employed for medical and technical applications. Solid-state NMR spectroscopy is devoted to the chemical analysis of

insoluble compounds, to the study of electronic structures in conducting systems, and generally to the characterization and investigation of structural and dynamic properties of solid systems.

Rotational dynamics

The rotational dynamics of organic guest molecules is most favorably studied by ^{2}H solid-state NMR spectroscopy, employing deuterated –CD groups as sensors.[50]

Solid-state deuterium NMR (^{2}H NMR) has been shown to be a powerful technique to probe the dynamics of organic molecules adsorbed in porous materials.[46,63–65] The ^{2}H NMR line shape is mainly determined by intramolecular quadrupolar interactions and is highly sensitive to the mode of molecular motion and its rate. Information about molecular motions is commonly extracted from the line shapes of polycrystalline powders by comparing the experimental spectra with a series of simulated spectra. In these simulations characteristic parameters such as the quadrupolar coupling constant, the asymmetry parameter, and the correlation rate, are varied.

The leading interaction in ^{2}H solid-state NMR is the quadrupolar interaction.[50,57] In the usual high field approximation, the first order quadrupolar interaction is characterized by two orientation dependent resonance frequencies ν_Q of the two spin transitions of the deuteron, given as:

$$\nu_Q(\vartheta,\varphi) = \pm Q_{zz}\frac{1}{2}(3\cos^2\vartheta - 1 - \eta\sin^2\vartheta\cos 2\varphi) \qquad (2)$$

Q_{zz} is a measure for the strength of the quadrupolar interaction. It corresponds to the largest frequency and the spectral width of possible frequencies is twice this value. The asymmetry parameter η is a measure of the deviation of quadrupolar interaction from axial symmetry. An alternative description of the strength of the quadrupolar interaction is the quadrupolar coupling constant, which for deuterons is given as $Q_{cc} = 4/3Q_{zz}$.

While in single crystals only two lines at $\pm\nu_Q$ are observable, the average over all possible orientations has to be calculated in a non-oriented powder sample. This integration gives the typical NMR powder line shapes, which are called the Pake pattern. For most organic CD groups a practically axial symmetric quadrupolar tensor with $\eta < 0.05$ and a value of $Q_{zz} \cong 120$–140 kHz is found. Because of the large spectral width, the ^{2}H-NMR spectra are measured with the solid echo sequence (Fig. 2(a)).

If the molecule undergoes fast re-orientations, the value of the quadrupolar tensor and thus also the quadrupolar coupling in general is changed, depending on the type and speed of the motion.[66] If the motions are fast on the NMR time scale, a relatively simple scenario is found: fast isotropic re-orientations of the benzene molecule, as for example in liquid benzene, cause a complete averaging of the quadrupolar tensor ($Q_{zz}^{iso} = 0$). Anisotropic rotations or rotational jump diffusions around the C_6-axis reduce the value of Q_{zz} to $Q_{zz}^{rot} = \frac{1}{2}Q_{zz}$. In these situations the normalized line shape of the solid echo spectrum is identical to the FID spectrum. In addition to these rotational motions there are often also librational motions which cause a partial reduction of the value of Q_{zz} at room temperature.

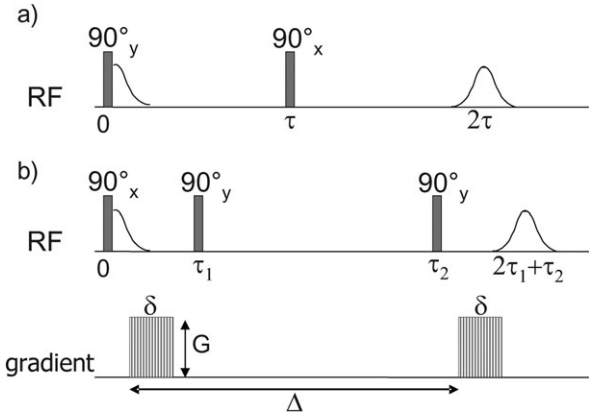

Fig. 2 Timing scheme of the (a) solid echo sequence for ^{2}H solid-state NMR spectroscopy and (b) stimulated echo sequence for the PFG experiments.

The situation is more complicated if the motions are not fast on the NMR time scale. In this case the line shape of the solid echo spectra depends very strongly on the echo delay time τ, and the distribution of rotational correlation times[67,68] Two limiting cases have to be considered, namely (a) the distribution function is very narrow (crystal-like behavior) and (b) the distribution function is very broad (glass-like behavior). In the crystal-like case the line shape of the solid echo spectra has to be calculated by standard NMR methods.[50] In the glass-like case however, the spectra are always a simple superposition of the slow and the fast limit spectra with varying weights.[68]

Translational dynamics

The effect of confinement and interaction with the large surfaces of these materials does not only affect the rotational but also the translational dynamics of guest molecules interacting with the pores. In particular, hydrogen bonding does not only influence molecular and intermolecular structures but can have also drastic effects on diffusion rates, as revealed by gradient NMR spectroscopy.[69–71] The main reason why these effects were discovered so relatively late is the fact that for most diffusing systems the surface to volume ratio of the pores is so small that molecules in direct contact to the surface are only a minor percentage of the overall molecules inside the pores. Thus the diffusion restrictions imposed on these molecules by hydrogen bonding are only of minor importance. However, in the mesoscopically structured porous silica this is no longer true and consequently the translational dynamics of guest molecules are strongly influenced by the porous environment.

The geometry of the pores is highly anisotropic and the pores' cylinder axis is the preferred direction of the diffusion. As a result of this the diffusion of guest liquids in the pores exhibits deviations from ordinary diffusion behavior.[72,73] In general, diffusion processes in porous media depend strongly on the type of the host and of the guest molecules. As a result of this dependence, different diffusion models for liquids and liquid guests in porous materials are discussed in the literature for various systems: ordinary diffusion,[74,75] restricted diffusion,[61,76] anisotropic diffusion,[60,77] and diffusion of different phases with individual diffusion coefficients.[78] All these models

differ more or less strongly from ordinary diffusion in isotropic systems such as bulk liquids. Anisotropic diffusion has been studied by NMR for various systems, as for example water between lamellar layers of a liquid crystal,[60] for salt-water ice,[79] and water in MCM-41.[77] Another possibility in the pores is a multi-phase scenario for the diffusion of guest molecules. Here the diffusion coefficients depend on the distance of the guest molecules from the surface, similar to the velocity profile of a laminar flow. Indications for such a behavior are found for example in water molecules interacting with protein surfaces.[61,80–85]

Diffusion processes are measured with NMR diffusometry, employing gradient techniques where a constant or pulsed magnetic field gradient in the direction of the external magnetic field is employed. The basics of diffusion in condensed matter are described for example in refs. 61 and 86 and are not repeated here. In the case of a constant gradient most experiments are performed in the stray field of a standard NMR magnet (stray field gradient, STRAFI NMR[87–93]) unless specialized anti-Helmholtz magnet systems with ultra high gradients are employed.[93] In both cases the experiment consists of three time periods. In the first period the initial spatial position is encoded *via* the position dependent Larmor frequency of the molecule; in the second period the molecule diffuses and changes its position; in the third period this change is revealed by determining the attenuation of the NMR signal caused by the diffusion (see Fig. 2(b)).

Chemical exchange

Finally also chemical exchange processes, for example between hydrogen donors on the surface and hydrogen acceptors on the guest molecules, are of importance for understanding the dynamical processes of the guest molecules in the vicinity of the surface. A detailed description of the influence of chemical exchange on NMR spectra is beyond the scope of this short review and can be found in the recent review articles by Bain[94] and some of us.[95] Here only the salient facts are given and we restrict here to first-order kinetics. The basic idea of this formalism is that the time scale of a chemical reaction or an exchange process is fast compared to the NMR time scale. Under this assumption the chemical reaction leads to a fluctuating time dependence of the chemical shift, *i.e.* the NMR frequency. It is permissible to treat the reaction as an instantaneous exchange between different static configurations, characterized by their static chemical shift, without having to take into account the actual reaction coordinates or pathway. In particular in the case of a fast exchange, where the exchange rates are much larger than the frequency differences, the result of the exchange is the weighted average of these static chemical shifts. As a simple example, let's assume that a proton is exchanging with rate constants k_{12} and k_{21} for the forward and backward reaction between two positions characterized by their Larmor frequencies ω_1 and ω_2. In the case of fast exchange $k_{21} \gg |\omega_1 - \omega_2|$ and/or $k_{21} \gg |\omega_1 - \omega_2|$ the average chemical shift is given as:

$$\bar{\omega} = \frac{k_{12}}{k_{12} + k_{21}}\omega_1 + \frac{k_{21}}{k_{12} + k_{21}}\omega_2. \qquad (3)$$

Results and discussions

Guest molecules with weak surface interactions

Benzene is an example of a molecule with weak surface interactions. As a result of this the effects of the surface will be mainly caused by the confinement and steric interactions with the surface. These effects are monitored by the rotational dynamics of the benzene molecule. In bulk benzene three states with different kinds of rotational motion can be distinguished by ^{2}H-NMR, namely a liquid state and two solid states: The first (liquid-like) state corresponds to fast isotropic rotational motions of the benzene molecule. The second (solid I) state is a fast anisotropic rotational jump diffusion around the six-fold axis. The third (solid II) state is the situation where all rotational motion appears frozen on the time scale of the ^{2}H solid-state NMR spectra, *i.e.* where the rotational correlation times are longer than *ca.* 1 ms. In the region of the solid I–solid II transition, where the rate of the 60° jump is comparable to quadrupolar frequencies, typical motion induced deviations from the common Pake pattern line shape are observed. These line shapes were reported by Vold and co-workers[67] for bulk benzene-d_6 and for benzene-d_6 confined in the cages of the cyclamer 1,3-cyclohexanedione.

From the properties of bulk benzene it is evident that also in the silica the frozen phase (solid II) is expected at temperatures well below 100 K. For glass-like systems of benzene however, a different behavior has been found.[96] Here a broad distribution of correlation times of the six-fold jump motion renders the spectra corresponding to the intermediate (solid I–solid II) invisible. This leads to spectra, which are a weighted superposition of spectra from molecules rotating slowly on the NMR time scale (solid II-like spectra) and spectra from molecules rotating fast on the NMR time scale (solid I-like spectra).

Fig. 3 compares the superposition of the experimental and simulated ^{2}H-NMR spectra of bulk benzene-d_6, benzene-d_6 inside the relatively narrow pores of SBA-15 (8 nm) and benzene-d_6 inside the mesoporous glass MCF with wide pores (30 nm) as a function of temperature. Comparing these spectra striking differences are visible. In the case of the bulk benzene (Fig. 3(a)) the temperature dependence reveals the typical line shapes of a crystal with well defined activation energies for the six-fold rotation as reported by Vold and co-workers.[67] This set of spectra serves as a landmark for the interpretation of the spectra of benzene inside the pores. The high temperature spectrum at 206.6 K shows the solid I spectrum of bulk benzene-d_6 with a strength of the quadrupolar interaction of 67 kHz. It represents the fast jump limit (high-temperature limit). In the temperature region between 130.2 and 107.0 K the jump rate is comparable to the NMR time scale and the typical effects on the line shape of the solid echo spectra[97] are visible. At 88.4 K the slow jump limit (low-temperature limit) is reached with the solid II spectrum with $Q_{zz} = 133$ kHz. From the simulation of the data the rate constants of the 60° jumps around the molecular axis as a function of the inverse temperature and from this the activation energy $E_a = 16.8$ kJ mol^{-1} and the pre-exponential factor $k_0 = 2.0 \times 10^{13}$ s^{-1} of the six-fold jump were determined.[20,67]

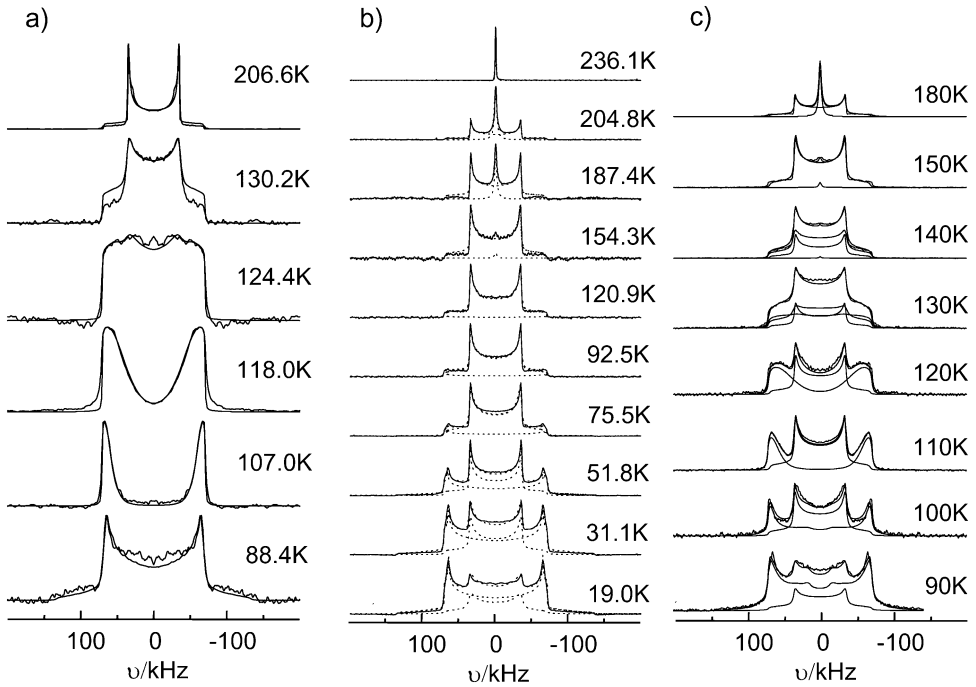

Fig. 3 ^{2}H-Solid-state NMR spectra of benzene-d_6. (a) Experimental and simulated crystalline bulk benzene in the temperature region where the transition from the pure solid II type (88.4 K) to the pure solid I type (206.6 K) spectrum occurs; all molecules have the same rotational correlation time, which reflects the crystalline order of the system. (b) Amorphous benzene inside mesoporous silica SBA 15 (pore diameter 8.0 nm); below 120 K the spectra are always the weighted superposition of the solid II and the solid I spectrum; starting at 154.3 K and above a narrow central line appears which is characteristic for liquid-like benzene. (c) Benzene inside mesoscopically organized controlled porous glass MCF (pore diameter 30 nm). Note that the spectra in (c) are decomposable into a crystalline component with spectra like (a) and an amorphous component like (b). (Figures adapted from data from refs. 20 and 46). From the intensity ratio of these two components the thickness of the amorphous surface layer is determinable.[46]

The ^{2}H-NMR spectra of benzene-d_6 in SBA-15 (Fig. 3(b)) are a superposition of two different components. In both components we note the absence of any signals characteristic for an intermediate rotational exchange regime in the ^{2}H-NMR spectra, *i.e.* spectra with the line shape of bulk benzene at temperatures in the range of 100–130 K. Here, the benzene molecules are found in two separate Pake subspectra of solid I and solid II type with temperature dependent relative concentrations. At higher temperatures most molecules are in the solid I-like state. Upon lowering of the temperature more and more of the benzene molecules are found in the solid II-like line. In particular there is no longer a well defined phase transition temperature for the freezing of the rotational motion. Similar behavior is found for the temperature range from 154 to 204 K. Here the spectra are a superposition of the solid I spectrum and the liquid-like narrow line. This is the typical behavior of a glass-like amorphous phase with a broad distribution of activation energies. This result shows that an amorphous benzene phase is formed inside the pores of SBA-15.

Fig. 3(c) displays the experimental ^{2}H-NMR spectra of benzene-d_6 confined in the pores of the mesoporous silica MCF in the temperature range between 90.1 and 180.3 K. At all temperatures the spectra exhibit a fairly complex line shape. Each spectrum represents a superposition of several sub-spectra with varying intensity ratios. A simulation of these spectra as a superposition of an inner crystalline and an amorphous surface benzene phase, characterized by superposition of solid I and solid II components with crystalline components from the intermediate regime, leads to an excellent reproduction of the experimental line shape, in particular for the spectra measured at 110 and 120 K.

From the intensities of the spectral components the relative numbers of molecules in the amorphous and crystalline phases can be determined. Employing the spectra at 110, 120 and 180 K the determined ratios are:[46] $I_{Core} : I_{Glass} = 0.82 : 0.18$ at 110 K, $I_{Core} : I_{Glass} = 0.79 : 0.21$ at 120 K and $I_{Core} : I_{Glass} = 0.77 : 0.23$ at 180 K, which coincide within the experimental error to an average value of $I_{Core} : I_{Glass} = 0.8 : 0.2$. Knowing the pore diameter it is possible to determine the thickness of the amorphous surface phase to 2–3 molecules of benzene from this value.

Guest molecules with strong surface interactions

The situation changes strongly when the guest molecules can exhibit strong surface interactions, as for example hydrogen bonds to the silanol groups. Here two limiting cases are of interest, namely molecules which interact only strongly with the surface, as for example pyridine, and molecules where interactions among themselves compete with the surface interaction, as for example in water.

Pyridine

In the case of pyridine the ring nitrogen is a strong hydrogen bond acceptor. As a result of this the pyridine interacts

strongly with the surface. The results of these interactions are most pronounced for low filling factors, where mainly a monolayer equivalent of pyridine molecules is inside the pores. In the case of pyridine a combination of several experimental techniques reveals the dynamic properties. From static ^{15}N-CP-NMR and ^{2}H-solid echo NMR of labeled pyridine (Fig. 4(a)–(e)) the rotational dynamics of the pyridine is revealed. Calculations of possible rotations reveal that the rotational motion of the adsorbed pyridine molecules (see Fig. 5(c)) is describable as a combined rotation around the Si–O bond (R_2) and an overall rotation (R_1) of the pyridine molecule, which is connected to a surface hopping process. A rotation around the OH···N hydrogen bond is not observed, presumably due to steric hindrance.[42] From the residual anisotropy of the NMR interaction tensors at high temperatures it is possible to elucidate a semi-quantitative model of the silica surface (Fig. 5(d)). While the smaller MCM-41 has relatively smooth surfaces, the large diameter SBA-15 is characterized by a rough surface with silica islands.[42]

The second rotation (R_1) is connected to the breaking and reformation of the hydrogen bond to the surface. Thus the motion of the pyridine molecules is a surface hopping, which results in a complicated interplay of rotational and translational motions (see Fig. 5(a)).

The translational diffusion of pyridine as a guest molecule inside mesoporous MCM-41 is studied with stray field gradient NMR for different filling factors of the pyridine (see Fig. 4(h)), ranging from a mono-molecular layer of pyridine on the inner surfaces of the pores to nearly completely filled pores.[20] The analysis of the resulting diffusion data reveals as expected a strongly anisotropic diffusion tensor. At a low filling factor of nominal 25%, which corresponds to a monolayer coverage, the principal components of the diffusion tensor are $D_{||} = 1.0 \times 10^{-9}\ m^2\ s^{-1}$ for the parallel and $D_{\perp} = 3.7 \pm 2.0 \times 10^{-11}\ m^2\ s^{-1}$ for the perpendicular component. While the perpendicular component is independent of the filling factor, the parallel component grows with the pore filling. This is an indication that at higher filling factors the diffusion is exchange mediated (see Fig. 5(b)). From ^{15}N-CP-MAS NMR (see Fig. 4(g) and (f)) it is evident that these exchange processes are fast on the NMR time scale.

Water

The situation is even more complicated if the guest molecule is water. The special physical and solvent properties of the water

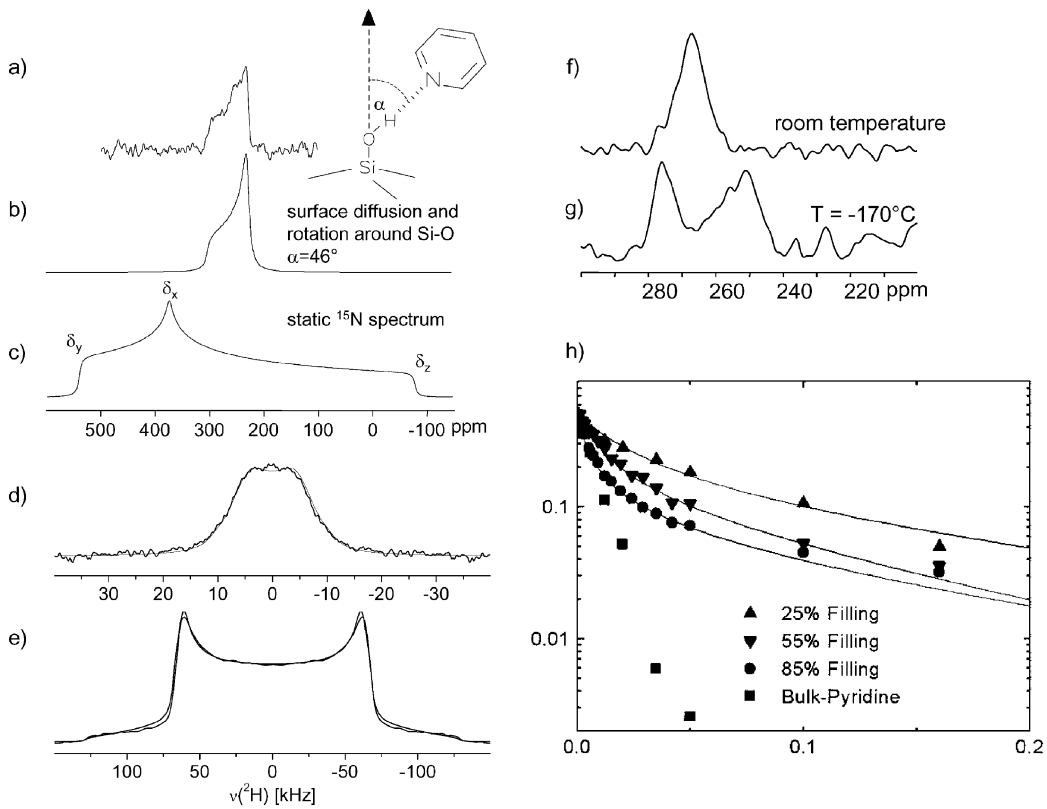

Fig. 4 Pyridine as a guest in mesoporous silica. (adapted from refs. 39 and 42): (a) The experimental room temperature ^{15}N-NMR spectrum obtained with cross polarization and high power proton decoupling reveals a residual anisotropy. The simulation (b) of the spectrum is employing the motional model described in Fig. 5(c) using an –SiOH···N angle of $\alpha = (49 \pm 2)^{\circ}$ and the ^{15}N CSA data from ref. 98 shown in (c). (d, e) Superposition of experimental and simulated ^{2}H-NMR solid-echo spectra of pyridine-4-d_1 as guest in MCM-41. The low-temperature (175 K) spectrum (e) exhibits the full size and anisotropy of a quadrupolar-CD tensor; the room-temperature spectrum (d) exhibits a reduced quadrupolar line width due to the molecular motions of the pyridine on the silica surface. The simulations are done as in (b). (f, g) Room-temperature and low-temperature CP-MAS NMR spectra of pyridine-^{15}N in silica. In the low-temperature spectrum (g) two lines are visible which correspond to free and hydrogen bound pyridine. In the room-temperature spectrum (f) only a single line is visible, which shows that all pyridine molecules are in fast exchange with each other.

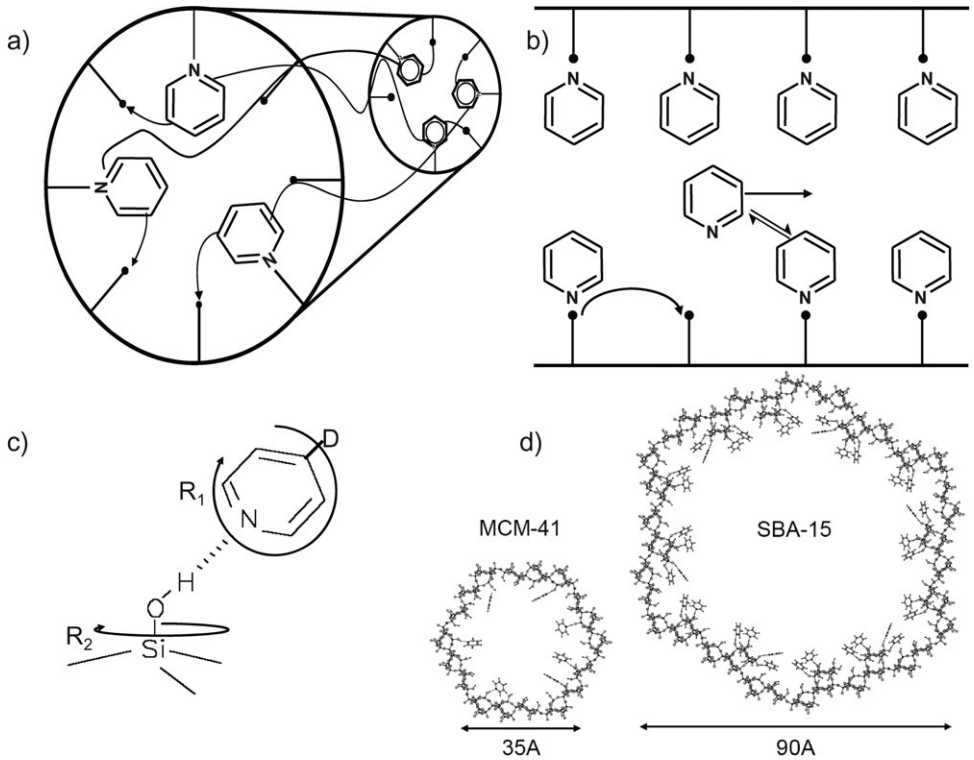

Fig. 5 (a) Surface hopping of pyridine adsorbed *via* hydrogen bonding on the surface of mesoporous silica, developed from Fig. 4. The motion is a superposition of translational diffusion (b), which is analyzed by NMR diffusometry[20] and rotational motion (c), which is analyzed by ^{15}N and ^{2}H line shape analysis.[42] From the rotational data a detailed model of the surface morphology is deduced.

stem largely from its extraordinary internal cohesiveness, compared to most other low molecular weight liquids. This cohesiveness is mainly the result of the water molecules high polarity and their ability to form hydrogen bonded networks among themselves, as for example in the frozen phase or in the bulk liquid phase. In restricted geometries the water molecules can also interact with the surfaces through hydrophobic and hydrophilic interactions and hydrogen bond interactions; hence there is a competition between the surface-liquid and liquid–liquid interactions. This competition leads to interesting new structures of water, as for example partial ordering of water molecules in the vicinity of the confining surface. Important examples of such systems are water molecules enclosed in porous media like zeolites[99] or cements,[100] or water molecules in hydration shells of proteins.[61,80–83,101,102] or bound water near the pore surface[26,103–113] or water clusters in narrow pores[114] or wells on nanoparticles.[115] Theoretical description of the behavior of water on silica surfaces is possible by the use of CPMD calculations.[116]

In the case of silica surfaces the water molecules are characterizable by virtue of their apparent chemical shifts. These chemical shifts are the result of an exchange of protons bound to the silica or water molecules. Fig. 6 displays the different possible scenarios of water molecules hydrogen bonded to the silica surface or among each other or free. Each scenario is characterized by an individual ^{1}H-chemical shift. While in principle these ^{1}H-chemical shifts are unique for a defined structure of the water interacting with the surface and other water molecules, in practice it must be taken into account that dynamic exchange effects such as molecular reorientations of the water molecules, rotations of the surface –SiOH groups and proton transfer, can and in general will, cause changes of these chemical shifts that lead to complete or full averaging of the line positions. Nevertheless it is still possible to distinguish between different environments and thus determine the relative amounts of the individual species by virtue of the ^{1}H-chemical shift, as discussed by Grünberg *et al*.[44]

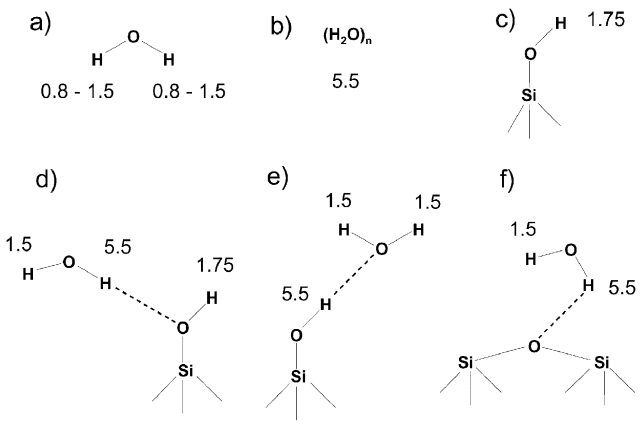

Fig. 6 Overview of possible –OH groups in the water/silica samples and the corresponding chemical shifts in ppm (TMS). Upper row: chemical shifts of the constituents of monomeric water, water clusters and silanol groups. Lower row: chemical shifts (adapted from refs. 44, 54, 117 and 118) observed in various hydrogen bonding scenarios.

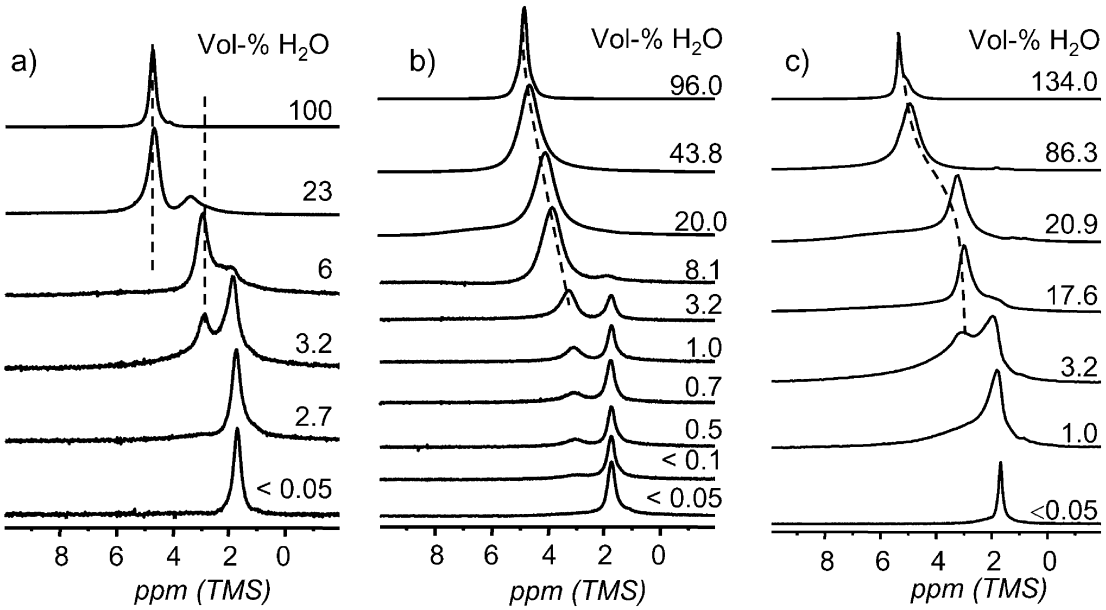

Fig. 7 Experimental ^{1}H-MAS solid-state NMR spectra (10 kHz) of water in (a) MCM-41, (b) SBA-15 and (c) CPG 10-75. Note the bimodal filling mechanism in the narrow pores of MCM-41 and the smooth variation of the CS in SBA-15 and CPG 10-75 (adapted from refs. 44 and 118).

Fig. 7 displays the ^{1}H-MAS-NMR spectra of water in MCM-41, SBA-15 and CPG 10-75 for different water contents recorded at a MAS frequency of 10 kHz. All presented spectra are normalized to their maximal intensity. The spectra, in general, exhibit several resolved lines with typical line-widths of (0.2–0.7) ppm. The ^{1}H-MAS-NMR spectrum which was measured after drying on the vacuum line exhibits a single line at $\delta = 1.74$ ppm in all samples. This single line is characteristic for surface silanol groups. However, even in the nominally completely dried sample some spectral intensity between two and three ppm in the SBA-15 and CPG 10–75 samples is observed.

This spectral intensity is evidence for strongly bound residual water molecules, which are probably stuck in the pore defects and hydrogen bonded to silica surface. This result is in contrast to the well ordered surface of MCM-41, where all water molecules are easily removable. Comparing the observed chemical shifts of the water signals at low filling levels (2.0–3.2 ppm) with the values given for the possible chemical shifts of –OH groups (see Fig. 6), it is evident that none of these shifts matches the observed shift. From this it follows that the observed shift is the result of a weighted averaging between different water species, which are in fast chemical exchange among themselves. Consequently all water molecules contribute to hydrogen bonds. Upon further increase of the water content two processes start: on the one hand the average of the line is low-field shifted towards the chemical shift values of water clusters and on the other hand the number of free surface –SiOH groups is reduced, which is visible as a decline in the intensity of the 1.74 ppm line. This process continues until the whole accessible surface is covered by a nominally monomolecular water layer. In the case of SBA-15, this happens at a water content of 8%. This corresponds to *ca*. 3.5 water molecules nm^{-2}. This shows that now all –SiOH groups are part of a hydrogen bonding network of exchanging hydrogen bonded protons (see Fig. 6).

Upon further increase of the water content, the silica systems behave differently. In the case of the narrow pore MCM-41, a bifurcation in the spectra (see 23% sample) occurs with two lines, one at the position of the monomolecular surface layer and the second at the position of a pore completely filled with water. In the case of the larger pores of CPG 10-75 and SBA-15 the line close to 3 ppm increases in intensity and shifts low-field towards the chemical shift values of water clusters. This indicates different pore filling mechanisms in the pores. The wide pores are filled layer wise starting at the pore wall and the narrow pores are filled axial *via* water droplets.

Binary mixtures

As was shown in the previous examples, already simple liquids inside mesoporous silica exhibit new structures and complex dynamics, which may differ strongly from the bulk behavior. Thus one can expect an even more complicated behavior if mixtures of several liquids are filled into the pores, in particular if the bulk mixtures of these liquids already exhibit a complicated phase behavior themselves. These effects were investigated by a binary mixture of water and isobutyric acid (iBA), a system with well-known bulk phase behavior. This has frequently been used as a model system in experimental studies of critical phenomena and phase separation in binary liquid mixtures. It is a representative example of "simple" water-containing systems, which have a lower miscibility gap, where the phase separation occurs at low temperatures (see Fig. 8(b)). Moreover it is a model for the large family of water-containing binary mixtures, and for their behavior in a hydrophilic porous matrix.

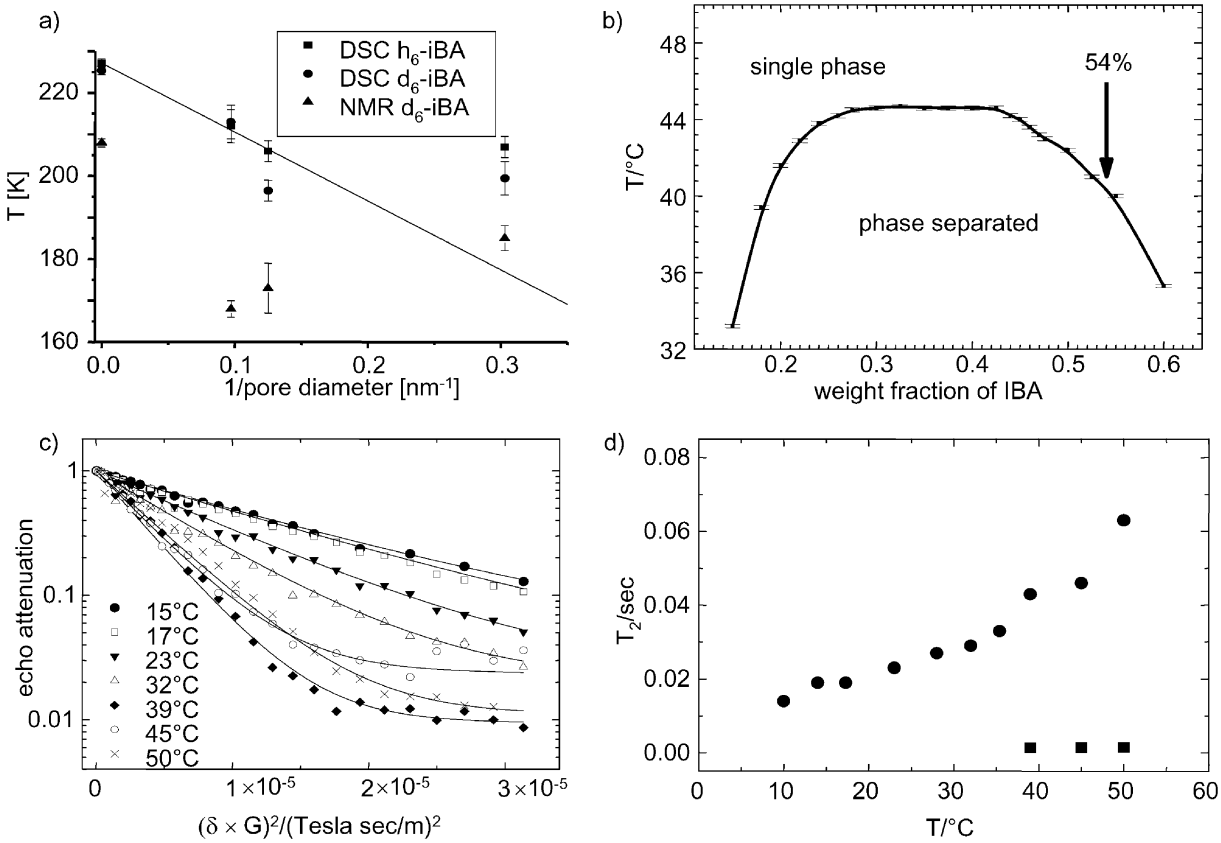

Fig. 8 Properties of pure isobutyric acid and water–isobutyric acid mixtures inside mesoporous silica. (a) Decoupling of rotational and translational melting point. (b) Phase diagram of the system isobutyric acid plus deuterated water (iBA/D_2O) (adapted from ref. 119). The arrow marks the composition studied in (Fig. 8c, 8d) as a guest inside the mesoporous silica. (c) Stimulated echo decay curves of iBA inside CPG 10-75 (experiment and calculation). Note that the fastest decay is observed for the 39 °C curve. This shows that the diffusion coefficient gets smaller above this temperature. (d) Temperature dependence of the spin–spin relaxation time T_2 in the confined mixture iBA/D_2O. The squares show the second component of spin–spin relaxation at high temperatures, which are attributed to immobilized iBA molecules, which are bound to the surface.

Before studying the binary mixture we investigate as a starting point the behavior of the pure iBA inside the pores.[49] Fig. 8(a) compares the temperatures of the melting of the translational degrees of freedom obtained by DSC with the melting temperatures of the rotational degrees of freedom obtained by ^{2}H solid-state NMR as a function of the inverse pore diameter. The full line indicates the Gibbs–Thomson equation with a constant C_{GT} = 80 K nm. Similar to the case of the benzene there are pronounced deviations of the data for iBA in MCM-41 from this relation. The rotational melting temperatures of d_6-iBA are 20 to 45 K lower than the respective thermodynamic melting temperatures T_m. These reductions of the melting points and the deviations from the Gibbs–Thomson equation indicate a strong interaction between the iBA molecules and the silica surface. In ref. 49 this deviation from the Gibbs–Thomson equation in MCM-41 is tentatively attributed to the strong binding of a monolayer of iBA molecules to the silica surface *via* hydrogen bonds. Owing to the amphipathic nature of the iBA-molecule, this renders the pore walls more hydrophobic than in the pristine state, such that the interaction of the second layer of molecules with the modified pore wall is grossly different. The consequences of this effect are clearly more pronounced for narrow pores (MCM-41) than in wider pores (CPG-10 and SBA-15).

This strong interaction between the iBA and the silica pores is also present in the case of the binary mixture.[119] The temperature dependence of the self-diffusion data (Fig. 8(c)) reveals a strong deviation from the Einstein behavior above 39 °C, where a slowdown of the diffusion is observed. This slowdown is the result of the binding of iBA molecules to the silica surface,[118] which is blocked for the iBA molecules at lower temperatures by water molecules. This interpretation is corroborated by the spin/spin relaxation data (Fig. 8(d)), which reveal the presence of immobilized iBA molecules with a very short T_2 at temperatures above 39 °C.

Discussion

As the previous examples from our group and many other research results worldwide have shown, the combination of various NMR techniques indeed provide the means for a full characterization of the behavior of guest molecules inside the pores of porous silica and related materials. These techniques reveal not only the basic physico-chemical properties of these molecules, but show also that the guest molecules exhibit new features which are not known for the bulk systems. These new features now naturally raise the question, what are typical effects of the confinement or the mesoscopic structure of the

system. From the experimental results on benzene and iBA inside the mesoporous silica two effects are evident, namely the reduction of the thermodynamic melting point and the decoupling of the rotational and translational degrees of freedom. For the first effect the Gibbs–Thomson equation is the commonly accepted explanation. However, as discussed above there are deviations from the Gibbs–Thomson equation, which show that even in relatively simple systems the thermodynamic behavior is not yet completely understood. Even more complicated is the behavior of the rotational melting temperature on the pore size. The size dependence on the temperature shows that new theoretical models are necessary for its understanding. A similar situation is found for the glass transition temperature in confined systems. Quoting the review of McKenna:[27] "*We survey the observations that show that the glass transition temperature decreases, increases, remains the same or even disappears depending upon details of the experimental (or molecular simulation) conditions. Indeed, different behaviors have been observed for the same material depending on the experimental methods used.*"

Taking into account that in the case of guest molecules inside the pores in general amorphous surface phases are formed, which exhibit glass-like dynamical behavior, one can at least speculate that both problems are related to similar physical phenomena and might be soluble by the same approach.

Conclusions

Employing solid-state NMR techniques it is nowadays easily feasible to study confined molecules, their mutual interactions and their interactions with the confining surface on a molecular level. From these studies it is possible to reveal the structure of the confined molecules inside the pores, their rotational and translational dynamics. These data now permit the development of a description of these confined systems which goes beyond the thermodynamic level.

Acknowledgements

Financial support by the DFG Sonderforschungsbereich SFB-448 is gratefully acknowledged.

References

1 J. S. Beck, J. C. Vartuli, W. J. Roth, M. E. Leonowicz, C. T. Kresge, K. D. Schmitt, C. T.-W. Chu, D. H. Olson, E. W. Sheppard, S. B. McCullen, J. B. Higgins and J. L. Schlenker, *J. Am. Chem. Soc.*, 1992, **114**, 10834.
2 A. Sayari and S. Hamoudi, *Chem. Mater.*, 2001, **13**, 3151–3168.
3 T. Linssen, K. Cassiers, P. Cool and E. Vansant, *Adv. Colloid Interface Sci.*, 2003, **103**, 121.
4 P. Selvam, S. K. Bhatia and C. G. Sonwane, *Ind. Eng. Chem. Res.*, 2001, **40**, 3237.
5 A. Schreiber, I. Ketelsen and G. H. Findenegg, *Phys. Chem. Chem. Phys.*, 2001, **3**, 1185.
6 F. Schüth and W. Schmidt, *Adv. Eng. Mater.*, 2002, **4**, 269–279.
7 A. Vinu, K. Z. Hossain and K. Ariga, *J. Nanosci. Nanotechnol.*, 2005, **5**, 347–371.
8 M. S. Morey, A. Davidson and G. D. Stucky, *J. Porous Mater.*, 1998, **5**, 195–204.
9 H. T. Chen, S. Huh, J. W. Wiench, M. Pruski and V. S. Y. Lin, *Abstr. Pap. Am. Chem. Soc.*, 2005, **229**, U983–U983.
10 H. T. Chen, S. Huh, J. W. Wiench, M. Pruski and V. S. Y. Lin, *J. Am. Chem. Soc.*, 2005, **127**, 13305–13311.
11 X. G. Wang, K. S. K. Lin, J. C. C. Chan and S. F. Cheng, *J. Phys. Chem. B*, 2005, **109**, 1763–1769.
12 A. Vinu, M. Miyahara and K. Ariga, *J. Nanosci. Nanotechnol.*, 2006, **6**, 1510–1532.
13 D. W. Aksnes and L. Gjerdaker, *J. Mol. Struct.*, 1999, **475**, 27.
14 F. Courivaud, E. W. Hansen, S. Kolboe, A. Karlsson and M. Stöcker, *Microporous Mesoporous Mater.*, 2000, **37**, 223.
15 H. Jobic, *Phys. Chem. Chem. Phys.*, 1999, **1**, 525.
16 V. Ladizhansky, G. Hodes and S. Vega, *J. Phys. Chem. B*, 2000, **104**, 1939.
17 Y. B. Mel,nichenko, J. Schüller, R. Richert, B. Ewen and C.-K. Loong, *J. Chem. Phys.*, 1995, **103**, 2016.
18 L. Gjerdaker, G. H. Sorland and D. W. Aknes, *Microporous Mesoporous Mater.*, 1999, **32**, 305.
19 E. W. Hansen, R. Schmidt, M. Stöcker and D. Akporiaye, *Microporous Mater.*, 1995, **5**, 143.
20 E. Gedat, A. Schreiber, J. Albrecht, I. Shenderovich, G. Findenegg, H. -H. Limbach and G. Buntkowsky, *J. Phys. Chem. B*, 2002, **106**, 1977.
21 R. Valiullin, S. Naumov, P. Galvosas, J. Kärger, H.-J. Woo, F. Porcheron and P. A. Monson, *Nature*, 2006, **443**, 965.
22 C. Alba-Simionesco, B. Coasne, G. Dosseh, G. Dudziak, K. Gubbins, R. Radhakrishnan and M. Sliwinska-Bartkowiak, *J. Phys.: Condens. Matter*, 2006, **18**, 15–68.
23 P. Medick, T. Blochowicz, M. Vogel and E. Rossler, *J. Non-Cryst.Solids*, 2002, **307**, 565–572.
24 G. Dosseh, Y. Xia and C. Alba-Simionesco, *J. Phys. Chem. B*, 2003, **107**, 6445.
25 S. A. Lusceac, C. Koplin, P. Medick, M. Vogel, N. Brodie-Linder, C. LeQuellec, C. Alba-Simionesco and E. A. Rossler, *J. Phys. Chem. B*, 2004, **108**, 16601–16605.
26 C. Favire, D. Bellet and G. Dolino, *Eur. Phys. J. B*, 1999, **7**, 19.
27 M. Alcoutlabi and G. B. McKenna, *J. Phys.: Condens. Matter*, 2005, **17**, R461–R524.
28 S. Kittaka, S. Ishimaru, M. Kuranishi, T. Matsuda and T. Yamaguchi, *Phys. Chem. Chem. Phys.*, 2006, **8**, 3223–3231.
29 L. D. Gelb, K. E. Gubbins, R. Radhakrishnan and M. Sliwinska-Bartkowiak, *Rep. Prog. Phys.*, 1999, **62**, 1573–1659.
30 M. Schoen and S. H. L. Klapp, *Nanoconfined Fluids. Soft Matter Between Two and Three Dimensions.*, John Wiley & Sons, New York, 2007.
31 M. Imperor-Clerc, P. Davidson and A. Davidson, *J. Am. Chem. Soc.*, 2000, **122**, 11925–11933.
32 L. A. Solovyov, O. V. Belousov, R. E. Dinnebier, A. N. Shmakov and S. D. Kirik, *J. Phys. Chem. B*, 2005, **109**, 3233–3237.
33 T. Hofmann, D. Wallacher, P. Huber, R. Birringer, K. Knorr, A. Schreiber and G. H. Findenegg, *Phys. Rev. B*, 2005, **72**, 064122.
34 G. A. Zickler, S. Jahnert, W. Wagermaier, S. S. Funari, G. H. Findenegg and O. Paris, *Phys. Rev. B*, 2006, **73**, 184109.
35 T. Shin, G. H. Findenegg and G. H. Brandt, *Prog. Colloid Polym. Sci.*, 2006, **133**, 116–122.
36 J. Trebosc, J. W. Wiench, S. Huh, V. S. Y. Lin and M. Pruski, *J. Am. Chem. Soc.*, 2005, **127**, 3057–3068.
37 J. Trebosc, J. W. Wiench, S. Huh, V. S. Y. Lin and M. Pruski, *J. Am. Chem. Soc.*, 2005, **127**, 7587–7593.
38 F. Stallmach, A. Graser, J. Kärger, C. Krause, M. Jeschke, U. Oberhagemann and S. Spange, *Microporous Mesoporous Mater.*, 2001, **44**, 745–753.
39 E. Gedat, A. Schreiber, G. Findenegg, I. Shenderovich, H.-H. Limbach and G. Buntkowsky, *Magn. Reson. Chem.*, 2001, **39**, 149.
40 L. Wasyluk, B. Peplinska, J. Klinowski and S. Jurga, *Phys. Chem. Chem. Phys.*, 2002, **4**, 2392–2397.
41 M. D. Jones, M. J. Duer, S. Hermans, Y. Z. Khimyak, B. F. G. Johnson and J. M. Thomas, *Angew. Chem., Int. Ed.*, 2002, **41**, 4726–4729.
42 I. Shenderovich, G. Buntkowsky, A. Schreiber, E. Gedat, S. Sharif, J. Albrecht, N. S. Golubev, G. H. Findenegg and H. H. Limbach, *J. Phys. Chem. B*, 2003, **107**, 11924–11939.
43 F. Babonneau, L. Yeung, N. Steunou, C. Gervais, A. Ramila and M. Vallet-Regi, *J. Sol–Gel Sci. Technol.*, 2004, **31**, 219–223.

44 B. Grünberg, T. Emmler, E. Gedat, I. Shenderovich, G. H. Findenegg, H. H. Limbach and G. Buntkowsky, *Chem.–Eur. J.*, 2004, **10**, 5689–5696.
45 Y. Komori and S. Hayashi, *Microporous Mesoporous Mater.*, 2004, **68**, 111–118.
46 W. Masierak, T. Emmler, E. Gedat, A. Schreiber, G. H. Findenegg and G. Buntkowsky, *J. Phys. Chem. B*, 2004, 18890–18896.
47 S. Pizzanelli, S. Kababya, V. Frydman, M. Landau and S. Vega, *J. Phys. Chem. B*, 2005, **109**, 8029–8039.
48 T. Azais, C. Tourne-Peteilh, F. Aussenac, N. Baccile, C. Coelho, J. Devoisselle and F. Babonneau, *Chem. Mater.*, 2006, **18**, 6382–6390.
49 A. Vyalikh, T. Emmler, I. Shenderovich, Y. Zeng, G. H. Findenegg and G. Buntkowsky, *Phys. Chem. Chem. Phys.*, 2007, **9**, 2249–2257.
50 K. Schmidt-Rohr and H. W. Spiess, *Multidimensional Solid State NMR and Polymers*, Academic Press, London, 1994.
51 R. Bohmer, G. Diezemann, G. Hinze and E. Rossler, *Prog. Nucl. Magn. Reson. Spectrosc.*, 2001, **39**, 191–267.
52 W. Paul and G. D. Smith, *Rep. Prog. Phys.*, 2004, **67**, 1117–1185.
53 L. Berthier, G. Biroli, J. P. Bouchaud, L. Cipelletti, D. El Masri, D. L'Hote, F. Ladieu and M. Pierno, *Science*, 2005, **310**, 1797–1800.
54 R. Anwander, I. Nagl, M. Widenmayer, G. Engelhardt, O. Groeger, C. Palm and T. Röser, *J. Phys. Chem. B*, 2000, **104**, 3532.
55 N. T. Whilton, B. Berton, L. Bronstein, H. -P. Hentze and M. Antonietti, *Adv. Mater.*, 1999, **11**, 1014.
56 A. Abragam, *Principles of Nuclear Magnetism*, Clarendon Press, Oxford, 1961.
57 C. P. Slichter, *Principles of Magnetic Resonance*, Springer Verlag, Berlin, Heidelberg, New York, 3rd edn, 1990.
58 R. Ernst, G. Bodenhausen and A. Wokaun, *Principles of NMR in One and Two Dimensions*, Clarendon Press, Oxford, 1987.
59 P. Mansfield and P. G. Morris, *NMR Imaging in Biomedicine*, Academic Press, New York, 1982.
60 P. T. Callaghan, *Principles of Nuclear Magnetic Resonance Microscopy*, Clarendon Press, Oxford, 1991.
61 R. Kimmich, *NMR Tomography Diffusometry Relaxometry*, Springer, Berlin, 1997.
62 M. Mehring, *High Resolution NMR Spectroscopy in Solids*, Springer Verlag, Berlin–Heidelberg–New York, 1983.
63 A. Stepanov, M. Alkaev, A. Shubin, M. Luzgin, T. Shegai and H. Jobic, *J. Phys. Chem. B*, 2002, **106**, 10114–10120.
64 D. W. Aksnes, L. Gjerdaker, L. Kimtys and K. Foerland, *Phys. Chem. Chem. Phys.*, 2003, **5**, 2680.
65 D. Aksnes and L. Kimtys, *Solid State Nucl. Magn. Reson.*, 2004, **25**, 146–152.
66 B. Boddenberg and R. Grosse, *Z. Naturforsch., A: Phys. Phys. Chem. Kosmophys.*, 1986, **41**, 1361.
67 J. H. Ok, R. R. Vold, R. L. Vold and M. C. Etter, *J. Phys. Chem.*, 1989, **93**, 7618.
68 E. Roessler, M. Taupitz, K. Börner, M. Schulz and H. M. Vieth, *J. Chem. Phys.*, 1990, **92**, 5847.
69 P. E. Hansen and S. Simon, *Magn. Reson. Chem.*, 1997, **35**, 320.
70 N. Tjandra and A. Bax, *J. Am. Chem. Soc.*, 1997, **119**, 8076.
71 G. S. Kapur, E. J. Cabrita and S. Berger, *Tetrahedron Lett.*, 2000, **41**, 7181.
72 J. Kärger and D. M. Ruthven, *Diffusion in Zeolites and Other Microporous Solids*, Wiley, New York, 1992.
73 F. J. Keil, R. Krishna and M.-O. Coppens, *Rev. Chem. Eng.*, 2000, **16**, 71.
74 E. L. Hahn, *Phys. Rev.*, 1950, **80**, 580–594.
75 D. E. Woessner, *J. Chem. Phys.*, 1961, **34**, 2057–2061.
76 J. Kärger, N.-K. Bär, W. Heink, H. Pfeifer and G. Seiffert, *Z. Naturforsch., A: Phys. Sci.*, 1994, **50**, 186–190.
77 F. Stallmach, J. Kärger, C. Krause, M. Jeschke and U. Oberhagemann, *J. Am. Chem. Soc.*, 2000, **122**, 9237–9242.
78 E. W. Hansen, R. Schmidt and M. Stöcker, *J. Phys. Chem.*, 1996, **100**, 11396.
79 M. I. Menzel, S.-I. Han, S. Stapf and B. Blümich, *J. Magn. Reson.*, 2000, **143**, 376–381.
80 R. Kimmich and H. W. Weber, *Phys. Rev. B*, 1993, **47**, 788.
81 R. Kimmich, F. Klammler, V. D. Skirda, I. A. Serebrennikova, A. I. Maklakhov and N. Fatkullin, *Appl. Magn. Reson.*, 1993, **4**, 425.
82 J. Bodurka, A. Gutsze, G. Buntkowsky and H.-H. Limbach, *Z. Phys. Chem.*, 1995, **190**, 99.
83 J. Bodurka, G. Buntkowsky, A. Gutsze and H.-H. Limbach, *Z. Naturforsch., C: Biosci.*, 1996, **51**, 81.
84 J. Bodurka, G. Buntkowsky, A. Gutsze and H.-H. Limbach, *Appl. Spectrosc.*, 1996, **50**, 1421.
85 A. Gutsze, J. Bodurka, R. Olechnowicz, G. Buntkowsky and H.-H. Limbach, *Z. Naturforsch., C: Biosci.*, 1995, **50**, 410.
86 J. Kärger, P. Heitjans and R. Haberlandt, *Diffusion in Condensed Matter*, Vieweg, Braunschweig/Wiesbaden, 1998.
87 M. Appel, G. Fleischer, J. Kärger, F. Fujara and I. Chang, *Macromolecules*, 1994, **27**, 4274–4277.
88 G. Fleischer and F. Fujara, *Macromolecules*, 1992, **25**, 4210–4212.
89 R. Kimmich, W. Unrath, G. Schnur and E. Rommel, *J. Magn. Reson.*, 1991, **91**, 136–140.
90 R. Kimmich, T. Zavada and S. Stapf, *Mater. Res. Soc. Symp. Proc.*, 1997, **464**, 313–324.
91 M. Ylihautala, J. Jokisaari, E. Fischer and R. Kimmich, *Phys. Rev. E*, 1998, **57**, 6844–6850.
92 S. Pahl, G. Fleischer, F. Fujara and B. Geil, *Macromolecules*, 1997, **30**, 1414–1418.
93 I. Chang, F. Fujara, B. Geil, G. Hinze, H. Sillescu and A. Tölle, *J. Non-Cryst. Solids*, 1994, **172–174**, 674–681.
94 A. D. Bain, *Prog. Nucl. Magn. Reson. Spectrosc.*, 2003, **43**, 63–103.
95 G. Buntkowsky and H. H. Limbach, *J. Low Temp. Phys.*, 2006, **143**, 55–114.
96 M. Schulz, A. van der Est, E. Roessler, G. Kossmehl and H. M. Vieth, *Macromolecules*, 1991, **24**, 5040.
97 H. W. Spiess and H. Sillescu, *J. Magn. Reson.*, 1981, **42**, 381.
98 D. Schweitzer and H. W. Spiess, *J. Magn. Reson.*, 1974, **15**, 529–539.
99 E. W. Hansen, M. Stöcker and R. Schmidt, *J. Phys. Chem.*, 1996, **100**, 2195–2200.
100 M. J. Setzer, *J. Colloid Interface Sci.*, 2001, **243**, 193.
101 J. Bodurka, G. Buntkowsky, R. Olechnowicz, A. Gutsze and H.-H. Limbach, *Colloids Surf., A*, 1996, **115**, 55.
102 J. Bodurka, G. Buntkowsky, A. Gutsze and W. Masierak, *Colloids Surf., A*, 1999, **158**, 115–119.
103 K. Overloop and L. van Gerven, *J. Magn. Reson., Ser. A*, 1993, **101**, 179.
104 K. Morishige and H. Iwasaki, *Langmuir*, 2003, **19**, 2808.
105 Y. Hirama, T. Takahashi, M. Nino and T. Sato, *J. Colloid Interface Sci.*, 1996, **184**, 349.
106 T. Ishizaki, M. Maruyama, Y. Furukawa and J. G. Dash, *J. Cryst. Growth*, 1996, **163**, 455.
107 E. W. Hansen, E. Tangstad, E. Myrvold and T. Myrstad, *J. Phys. Chem. B*, 1997, **101**, 10709.
108 K. Morishige and K. Nobuoka, *J. Chem. Phys.*, 1997, **107**, 6965.
109 J. M. Baker, J. C. Dore and P. Behrens, *J. Phys. Chem. B*, 1997, **101**, 6226.
110 T. Takamuku, M. Yamagami, H. Wakita, Y. Masuda and T. Yamaguchi, *J. Phys. Chem. B*, 1997, **101**, 5730.
111 K. Morishige and K. Kawano, *J. Chem. Phys.*, 1999, **110**, 4867.
112 J. Dore, *Chem. Phys.*, 2000, **258**, 327.
113 E. Liu, J. C. Dore, J. B. W. Weber, D. Khushalani, S. Jahnert, G. H. Findenegg and T. Hansen, *J. Phys.: Condens. Matter*, 2006, **18**, 10009–10028.
114 M. Febles, N. Perez-Hernandez, C. Perez, M. L. Rodriguez, C. Foces-Foces, M. V. Roux, E. Q. Morales, G. Buntkowsky, H. H. Limbach and J. D. Martin, *J. Am. Chem. Soc.*, 2006, **128**, 10008–10009.
115 S. Bhosale, G. T. Li, F. T. Li, T. Y. Wang, R. Ludwig, T. Emmler, G. Buntkowsky and J. H. Fuhrhop, *Chem. Commun.*, 2005, 3559–3561.
116 C. Mischler, J. Horbach and W. K. Binder, *J. Phys.: Condens. Matter*, 2005, **17**, 4005–4013.
117 M. Nakahara and C. Wakai, *Chem. Lett.*, 1992, 809–812.
118 A. Vyalikh, T. Emmler, B. Grünberg, Y. Xu, I. Shenderovich, G. H. Findenegg, H.-H. Limbach and G. Buntkowsky, *Z. Phys. Chem.*, 2007, **221**, 155–168.
119 A. Vyalikh, T. Emmler, E. Gedat, I. Shenderovich, G. H. Findenegg, H.-H. Limbach and G. Buntkowsky, *Solid State Nucl. Magn. Reson.*, 2005, **28**, 117–124.